

---

# How Focused Are LLMs? A Quantitative Study via Repetitive Deterministic Prediction Tasks

---

**Wanda Hou**  
EdenCode Inc.  
hwanda@edencode.ai

**Leon Zhou**  
Stevenson School  
lzhou26@stevensonschool.org

**Hong-Ye Hu**  
Harvard University  
hongyehu@fas.harvard.edu

**Yubei Chen**  
UC Davis  
ybchen@ucdavis.edu

**Yi-Zhuang You**  
EdenCode Inc.  
zyyou@edencode.ai

**Xiao-Liang Qi**  
Path Integral Technology, Inc.  
phynics@pathintegral.xyz

## Abstract

We investigate the performance of large language models (LLMs) on repetitive deterministic prediction tasks and study how the sequence accuracy rate (SAR) scales with output length. Each such task involves the repetition of the same operation  $n$  times. Examples of such tasks include letter replacement in letter strings following a given rule, integer addition, and multiplication of string operators in many-body quantum mechanics. If the LLM performs the task by a simple repetition algorithm, the success rate would follow an exponential decay with sequence length. In contrast, our experiments on leading LLMs reveal a sharp double-exponential drop beyond a characteristic length scale—an accuracy cliff marking a transition from reliable to unstable generation. This implies that LLMs fail to execute each operation independently. To explain this phenomenon, we propose a statistical-physics-inspired model capturing the competition between external conditioning from the prompt and internal interference among generated tokens. The model quantitatively reproduces the observed crossover and provides an interpretable link between attention-induced interference and sequence-level failure. Fitting the model to empirical results across multiple LLMs and tasks yields effective parameters that characterize the intrinsic error rate and error accumulation factor for each model-task pair, offering a principled framework for understanding the limits of deterministic accuracy in LLMs.

## 1 Introduction

*Accuracy rate* is among the most fundamental and widely adopted evaluation metrics in machine learning, especially for classification and other discriminative tasks. Its appeal lies in the clarity of its definition: each input has a well-defined ground-truth label, and the model’s prediction can be judged unambiguously as correct or incorrect. This binary criterion makes accuracy a natural measure of performance, enabling direct comparison across models and datasets.

However, this paradigm does not directly extend to large language models (LLMs). Many LLM applications, such as machine translation, summarization, or dialogue, are inherently sequence-to-

sequence generation problems. In these settings, the model generates text probabilistically, token by token, sampling from a distribution of plausible continuations. Crucially, there is rarely a single “correct” output: multiple valid translations, summaries, or conversational responses may exist. Consequently, simple exact-match accuracy is insufficient for evaluation, and researchers rely instead on a suite of task-specific metrics (e.g., BLEU, ROUGE, perplexity, or human judgment) [Papineni et al., 2002, Lin, 2004, Liang et al., 2022] that capture fluency, coherence, and relevance.

Yet this limitation is context-dependent. In scientific domains—including mathematics, physics, and computer science—the nature of the task often changes. Here, many problems admit a unique correct solution: a definite numerical value, a closed-form expression, or a precise code output. For instance, the question “what is  $2342342 + 3442342$ ” has only one acceptable answer, and the model’s response must exactly match the correct sequence of digits to be considered correct [Cobbe et al., 2021, Hendrycks et al., 2021, Lewkowycz et al., 2022]. In such applications, the probabilistic flexibility of LLMs does not diminish the importance of exact correctness. The evaluation once again reduces to a binary criterion: either the model outputs the correct sequence or it does not.

This observation motivates the introduction of a new evaluation concept tailored for LLMs in scientific applications: the *Sequence Accuracy Rate (SAR)*. SAR measures the proportion of problem instances for which the LLM produces the exact correct sequence as output. By aligning the evaluation of LLMs with the well-established standard of accuracy in classification, SAR provides a rigorous and interpretable metric for assessing LLMs in domains where precision and correctness are paramount, as illustrated in Fig. 1.

LLMs have achieved remarkable progress across a wide range of tasks, yet their reliability on structured, multi-step reasoning remains poorly understood [Wei et al., 2022, Havrilla et al., 2024]. While in generative modeling the challenge has often been framed as a tradeoff between diversity and realism [Astolfi et al., 2024], multi-step reasoning tasks demand consistent correctness across sequential subtasks. Success in these settings is inherently *factorizable*: the probability of solving the overall problem is the product of per-step accuracies, making performance highly sensitive to individual step error rates. This exposes whether models can exploit compositional structure rather than treating complex problems monolithically [Lake and Baroni, 2018].

To probe this challenge, we introduce a minimal and fully deterministic evaluation class where each problem instance admits a unique ground-truth solution and complexity can be tuned by a single parameter  $N$ . We present three complementary benchmarks: (i) *cyclic letter replacement task*, a purely symbolic problem over a finite alphabet that isolates stepwise error propagation without memory; (ii) *integer addition*, which tests the handling of local carry rules and long-range carry propagation across digits; and (iii) *Pauli string multiplication*, which requires tracking both local symbol rules and a global phase factor, thereby testing the model’s ability to maintain a lightweight memory across many steps. All three benchmarks share the key property that overall complexity decays multiplicatively with sequence length  $N$ , providing a clean probe of cumulative error accumulation in deterministic reasoning [Wang et al., 2022, Liu et al., 2023, Turpin et al., 2023, Wan et al., 2025a].

Beyond empirical evaluation, we develop a statistical physics interpretation of the observed behavior of SAR, drawing an analogy to the Ising model to assuming token correctness influence each other in random manner. Our theoretical model reproduces the accuracy-cliff cross-over behavior observed in LLMs, aligning closely with observed scaling behaviors, offering principled intuition for the limits of reliability as complexity grows. Together, our benchmarks and theoretical framework establish a controlled setting for studying how LLMs manage compositional reasoning, memory, and robustness in deterministic problem families.

## 2 Experiment

We prompted a set of large language models (LLMs)—gpt-5, gemini-2.5-pro, gemini-2.5-flash, grok-4, and claude-4-sonnet—to perform a series of deterministic sequence prediction tasks that each admit a unique correct solution. These tasks provide a well-defined setting for evaluating the sequence accuracy rate (SAR), enabling a quantitative analysis of how the accuracy of generated sequences scales with the problem size, measured by the output sequence length. During evaluation, all models were tested in a closed setting with external tools such as code execution and web access explicitly disabled, ensuring that results reflect the models’ internal reasoning capabilities only. While the quantitative results may vary slightly with prompt

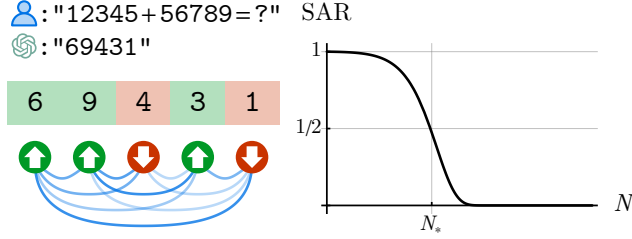


Figure 1: Illustration of the experimental setup and theoretical framework. The left panel shows examples of deterministic sequence prediction tasks (e.g., arithmetic problems) used to evaluate large language models (LLMs), where each token’s correctness is represented by a binary variable (Ising spin). Token errors are modeled as Ising spins interacting through all-to-all random couplings, capturing how correlations and noise propagate during sequence generation. The right panel displays the typical behavior of the Sequence Accuracy Rate (SAR) (i.e. the probability for all tokens to be correct in a output sequence) as a function of the sequence length  $N$ : SAR remains high for short sequences, then drops sharply beyond a characteristic crossover scale  $N_*$ , forming the accuracy cliff, which is nicely reproduced by a spin-glass statistical-mechanical model.

phrasing or instruction style, the qualitative behaviors reported here are robust across formulations. The prompt templates used for each task are available in the source code at [GitHub](#).

## 2.1 Cyclic Letter Replacement

We start with a simple *cyclic letter replacement* task defined over an alphabet

$$\mathcal{A} = \{A, B, C, \dots\}. \quad (1)$$

Each letter is mapped to an integer index  $x \in \{0, 1, \dots, |\mathcal{A}| - 1\}$ . The transformation rule is a cyclic shift by one modulo the alphabet size:

$$y = (x + 1) \bmod |\mathcal{A}|. \quad (2)$$

The output is then mapped back to a letter in  $\mathcal{A}$ . Each position in the input string is transformed independently, so for a string of length  $N$  the task is simply to apply the shift rule to each site.

Formally, given an input string

$$S = (x_1, x_2, \dots, x_N), \quad x_j \in \{0, \dots, |\mathcal{A}| - 1\}, \quad (3)$$

the transformed output string is

$$T = ((x_1 + 1) \bmod |\mathcal{A}|, (x_2 + 1) \bmod |\mathcal{A}|, \dots, (x_N + 1) \bmod |\mathcal{A}|). \quad (4)$$

For example, for  $\mathcal{A} = A, B, C, D$ :

$$\begin{aligned} \text{Input: } & \text{ADBAA} \Rightarrow \text{Output: } \text{BACBB} \\ \text{Input: } & \text{DABDC} \Rightarrow \text{Output: } \text{ABCAD} \end{aligned}$$

For this task, the results are presented in Fig. 2 and Fig. 3. Fig. 2 shows results from `gemini-2.5-pro` and `gemini-2.5-flash` with alphabet sizes  $|\mathcal{A}| = 4, 9, 13, 26$ . Fig. 3 compares `gpt-5`, `gemini-2.5-pro`, `gemini-2.5-flash`, `grok-4`, and `claude-4-sonnet` at  $|\mathcal{A}| = 13$ .

## 2.2 Integer Addition

Next, we consider *integer addition* with a fixed number of digits. The task probes arithmetic consistency and multi-digit carry propagation—requiring sequential reasoning rather than purely single-site transformations.

Each query presents an addition problem of the form

$$A + B, \quad (5)$$

where  $A, B \in \mathbb{N}$  are positive integers with the same digit lengths. The model is asked to compute the sum and return the result as a plain numeric string.

For example at  $N = 4$ :

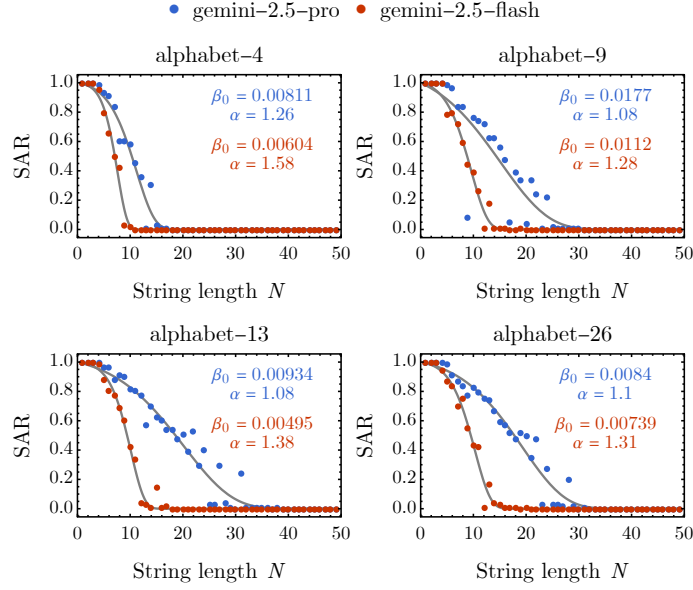


Figure 2: Cyclic letter replacement benchmark on gemini-2.5-pro and gemini-2.5-flash with alphabet size  $|\mathcal{A}| = 4, 9, 13$  and 26.

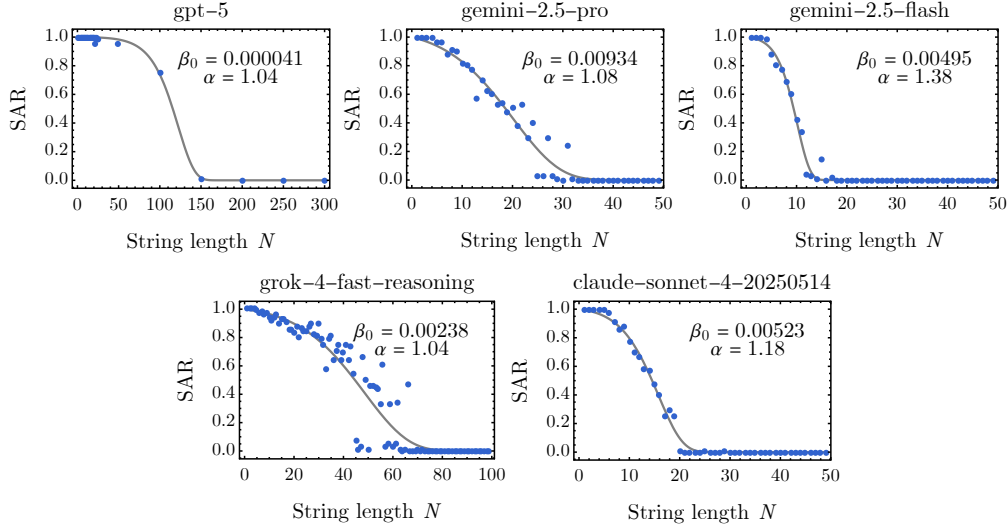


Figure 3: Cyclic letter replacement with alphabet size  $|\mathcal{A}| = 13$  across many different models.

Input: 1234 + 5678  $\Rightarrow$  Output: 6912  
 Input: 9999 + 0001  $\Rightarrow$  Output: 10000

The corresponding results are shown in Fig. 4, evaluating gemini-2.5-flash, gemini-2.5-pro, grok-4, and claude-4-sonnet.

### 2.3 Pauli Algebra

As a third deterministic benchmark, we consider *Pauli string multiplication* task with tunable string length. The Pauli operators  $X$ ,  $Y$ , and  $Z$  are  $2 \times 2$  matrices

$$X = \begin{pmatrix} 0 & 1 \\ 1 & 0 \end{pmatrix}, Y = \begin{pmatrix} 0 & -i \\ i & 0 \end{pmatrix}, Z = \begin{pmatrix} 1 & 0 \\ 0 & -1 \end{pmatrix}, \quad (6)$$

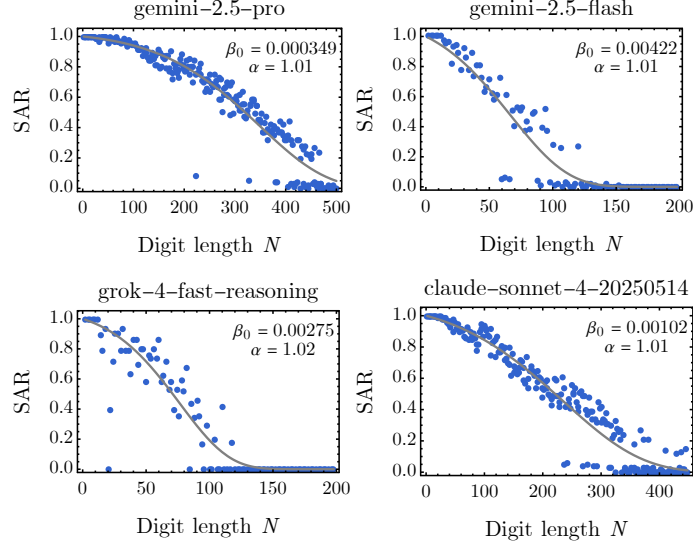


Figure 4: Integer addition benchmark across different models.

They originate as generators of the Lie algebra  $\mathfrak{su}(2)$ , up to constants. For our purposes we treat them algebraically, using only their multiplication rules and phase factors. The identity operator is denoted  $I$ . The single-qubit multiplication rules are

$$X \times X = Y \times Y = Z \times Z = I, \quad (7)$$

$$X \times Y = iZ, \quad Y \times X = -iZ, \quad (8)$$

$$Y \times Z = iX, \quad Z \times Y = -iX, \quad (9)$$

$$Z \times X = iY, \quad X \times Z = -iY, \quad (10)$$

together with  $I \times P = P$  for  $P \in \{I, X, Y, Z\}$ .

A Pauli string on  $N$  sites is

$$S = \alpha \bigotimes_{\ell=1}^N P_{\ell}, \quad (11)$$

where  $\alpha \in \{\pm 1, \pm i\}$  is a global phase and  $P_{\ell} \in \{I, X, Y, Z\}$ . Because Pauli operators acting on different sites commute, the product of two strings reduces to independent local multiplications together with accumulation of the global phase:

$$\left( \alpha_1 \bigotimes_{\ell=1}^N P_{\ell} \right) \left( \alpha_2 \bigotimes_{\ell=1}^N Q_{\ell} \right) = \left( \alpha_1 \alpha_2 \prod_{\ell=1}^N \phi_{\ell} \right) \bigotimes_{\ell=1}^N R_{\ell}, \quad (12)$$

where  $P_{\ell} \times Q_{\ell} = \phi_{\ell} R_{\ell}$  with  $\phi_{\ell} \in \{\pm 1, \pm i\}$  and  $R_{\ell} \in \{I, X, Y, Z\}$ .

This structure makes the task explicitly factorizable: each site requires a local Pauli multiplication and a phase update, while the overall result depends on consistent accumulation of all local outcomes. See Sec. A for a theoretical complexity analysis.

The need to consistently maintain and update the global phase highlights the role of *memory handling* in multi-step reasoning. Unlike purely sitewise problems, errors here can accumulate not only locally but also through the global phase register.

For this task, the results are presented in Fig. 5, evaluating `gemini-2.5-pro` and `gemini-2.5-flash` under two evaluation criteria: one requiring both the operator sequence and accumulated phase to be correct, and a relaxed criterion considering only the operator sequence while ignoring phase errors.

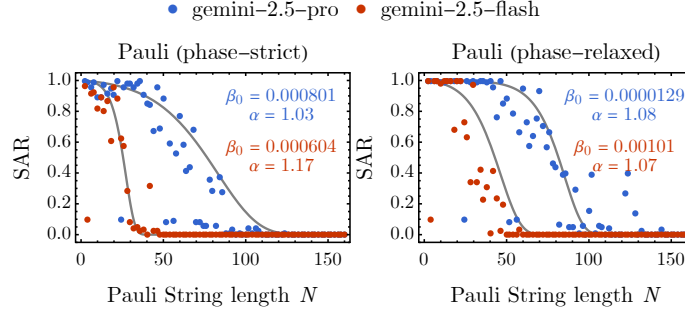


Figure 5: Pauli string multiplication benchmark on gemini-2.5-pro and gemini-2.5-flash evaluated under strict (phase-matched) and relaxed (phase-ignored) criteria.

### 3 Analysis

#### 3.1 Empirical Formula

In our experiments, we observed that the Sequence Accuracy Rate (SAR) depends strongly on the output sequence length  $N$ . Assuming independent per-token error events during generation, the baseline expectation is that the sequence accuracy rate decays exponentially with the sequence length  $N$ :

$$\text{SAR}(N) = e^{-\beta N}, \quad (13)$$

where  $\beta > 0$  denotes a constant per-token error rate. However, as we have seen in the above experiments, the empirical results deviate significantly from this simple picture. Instead of a smooth exponential decay, SAR exhibits a distinct crossover behavior: it remains nearly perfect for short sequences and then undergoes a rapid drop to zero around a characteristic length scale  $N_*$ .

This observation indicates that token errors are not independent: earlier tokens affect the error rate of subsequent tokens. To capture this history dependence, we treat the per-token error rate as a function of the sequence length  $N$  rather than a constant and adopt the following empirical fit:

$$\text{SAR}(N) = e^{-\beta(N)N}, \quad \beta(N) = \beta_0 \alpha^{N-1}, \quad (14)$$

where  $\beta_0 > 0$  quantifies the *intrinsic* error rate, and  $\alpha$  represents the *error accumulation factor*, which characterizes how local errors compound as the sequence length increases. When  $\alpha = 1$ , the model reduces to the standard exponential decay expected from independent token errors. For  $\alpha > 1$ , however, the effective error rate  $\beta(N)$  grows exponentially with  $N$  even when  $\beta_0$  is small, leading to a rapid, catastrophic drop in accuracy once  $\beta(N)$  becomes of order one. The onset of this accuracy cliff occurs at a characteristic sequence length

$$N_* \simeq 1 + \frac{\log(1/\beta_0)}{\log \alpha}, \quad (15)$$

beyond which scale the model’s reliability collapses.

#### 3.2 Hypothesis and Statistical Model

Empirically, the observed crossover length  $N_*$  is typically on the order of  $10 \sim 100$ —well within the attention window ( $\sim 10^5$  or larger) of modern LLMs. This rules out limited context length as the primary cause of the accuracy cliff. We therefore hypothesize that the rapid accuracy degradation arises intrinsically from the all-to-all coupling structure of the self-attention mechanism. While the attention weights in next-token prediction are structured and typically sparse rather than uniformly distributed over all past tokens, the architecture nonetheless enables fluctuations and errors to spread through the network in an effectively all-to-all fashion, propagating globally across the entire generated sequence. As a result, small local errors can be amplified and spread through these dense interactions, effectively inducing collective fluctuations among token-level accuracies.

To analyze this mechanism, we abstract away token content and focus solely on whether each token is generated correctly. We introduce binary variables  $s_i = \pm 1$  to represent the correctness of the  $i$ -th

token, with  $s_i = +1$  for correct and  $s_i = -1$  for incorrect generation. We model the joint distribution of token errors  $s = \{s_i\}$  using an effective Ising-like energy function,

$$E_J[s] = - \sum_{i < j} J_{ij} s_i s_j - h \sum_i s_i, \quad (16)$$

where  $h$  denotes an external field reflecting the baseline bias from the prompt toward correct generation, and  $J_{ij}$  represent effective couplings between token correctness variables. In the independent-token limit,  $J_{ij} = 0$  and the model will predict the exponential decay SAR following Eq. (13). However, experimental results described by Eq. (14) clearly indicate deviations from this independent picture, implying the presence of correlations among token outcomes.

We attribute these correlations to noisy, attention-induced interactions that can be modeled as random couplings drawn independently from a Gaussian ensemble,

$$\mathbb{E}_J[J_{ij}] = 0, \quad \mathbb{E}_J[J_{ij}^2] = J_0^2, \quad (17)$$

where  $J_0$  characterizes the strength of internal interference or “noise coupling.” The random couplings capture how attention-mediated dependencies introduce both constructive and destructive interference among tokens. Together with the external field  $h$ , which sets the intrinsic per-token accuracy, this formulation defines a statistical-physics model for the collective behavior of token errors. The model is mathematically equivalent to the Sherrington–Kirkpatrick (SK) spin-glass model, widely studied in statistical physics.

For a given realization of the couplings  $J_{ij}$ , the probability of observing a sequence of token correctness variables  $s$  is

$$p_J[s] = \frac{1}{Z_J} e^{-E_J[s]}, \quad (18)$$

with the partition function

$$Z_J = \sum_s e^{-E_J[s]}. \quad (19)$$

In particular, the SAR is associated with the probability of generating the fully correct sequence  $s = (1, 1, \dots, 1)$ , averaged over disorder realizations of the couplings. Using the geometric mean to account for multiplicative scaling, we define

$$\text{SAR} := \exp\left(\mathbb{E}_J[\log p_J[s = 1]]\right). \quad (20)$$

Under a perturbative approximation Sec. B, the solution of Eq. (20) takes the same form as the empirical law in Eq. (14), with empirical parameters  $\alpha, \beta_0$  related to the energy model parameters  $J_0, h$  as follows:

$$\alpha \simeq e^{\frac{2J_0^2}{1+2J_0}}, \quad \beta_0 = e^{-2h}. \quad (21)$$

From the statistical-physics perspective, the accuracy cliff corresponds to a finite-size crossover in the underlying spin system. For small system size  $N$ , the external field  $h$  dominates, and the system behaves as a paramagnet, aligning most spins in the correct direction ( $s_i = +1$ ). As  $N$  increases, however, the collective spin correlation energy from the random couplings  $J_{ij}$ , which scales as  $N^2$ , eventually exceeds the entropic contribution that grows only linearly with  $N$ . Beyond a characteristic size  $N_*$ , the interaction energy dominates, and the system crosses over into a spin-glass-like regime, where the fully aligned configuration is no longer favored, leading to the rapid accuracy degradation observed as the accuracy cliff.

Using the fitted results of the numerical data based on the form in Eq. (14), we pin each model onto the correlation–error map. This mapping translates observed SAR decay profiles into quantitative measures of intrinsic error rate and correlation strength, enabling direct comparison of how different LLMs accumulate and propagate errors across tasks. Each point on the map represents a model’s performance under a specific task, corresponding to a pair  $(\log \alpha, \log \beta_0)$  with color indicating  $\log N_*$ , where  $N_*$  is defined as the solution of  $\text{SAR}(N_*) = 0.5$  under the given parameters. A smaller  $\log \alpha$  means the model has a sharper focus of attention, and a smaller  $\log \beta_0$  means the model has a lower error rate for executing a single unit task. The mapping results grouped by model are shown in Fig. 6, and those grouped by task are shown in Fig. 7.

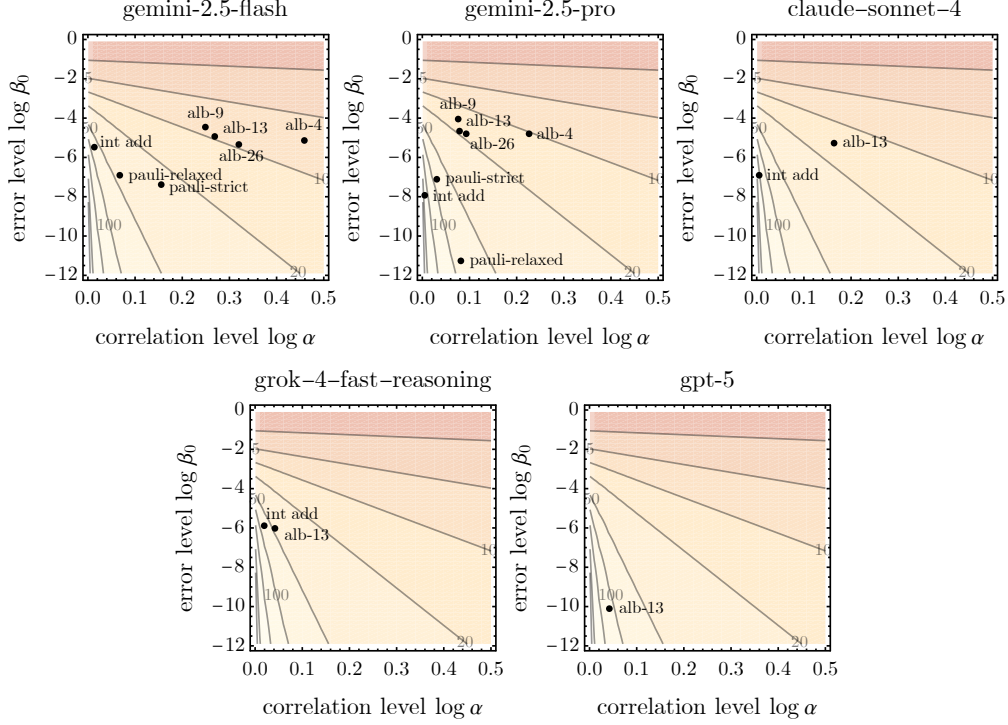


Figure 6: Correlation–error map grouped by model, with color indicating the value of  $\log N_*$ . The horizontal and vertical axes,  $(\log \alpha, \log \beta_0)$ , represent the correlation level and error level, respectively. The gray contour line and the numbers along it denote the sequence length  $N$ .

#### 4 Implication: Divide-and-Conquer Strategy

The empirical scaling law of Eq. (14) not only provides a qualitative description of how the accuracy inevitably degrades with the output sequence length  $N$  for LLMs, but also offers a *constructive implication*: when  $\alpha > 1$ , the reliability of long-sequence generation can be improved by adopting a *divide-and-conquer* strategy.

In this context, divide-and-conquer refers to partitioning a sequence-generation task of total length  $N$  into  $k$  sub-tasks of length  $N/k$ , prompting the model separately for each sub-task, and then merging the partial outputs to form the complete sequence. The intuition is that the observed accuracy cliff originates from correlated error propagation among tokens: when  $\alpha > 1$ , the effective per-token error rate grows exponentially with  $N$ , driven by all-to-all dependencies in the attention mechanism. Dividing the sequence into shorter fragments effectively *cuts the correlation loops*, preventing the catastrophic error accumulation.

We introduce a multiplicative overhead factor  $\theta_{N,k} \in (0, 1]$  to account for the reduction of SAR due to the additional operations involved in applying the divide-and-conquer strategy, such as segmentation, formatting, boundary handling, and content copying.  $\theta_{N,k}$  is expected to only depend on  $N$  and  $k$  weakly. The overall success probability under divide-and-conquer is then

$$\text{SAR}_{\text{DC}}(N, k) = \theta_{N,k} [\text{SAR}(N/k)]^k = \theta_{N,k} \exp \left[ -\beta_0 N \alpha^{\frac{N}{k}-1} \right]. \quad (22)$$

Define the logarithmic gain of divide-and-conquer relative to the single-shot strategy as

$$\Delta(N, k) := \log \frac{\text{SAR}_{\text{DC}}(N, k)}{\text{SAR}(N)} = \log \theta_{N,k} + \beta_0 N \left( \alpha^{N-1} - \alpha^{\frac{N}{k}-1} \right). \quad (23)$$

This formulation shows that for  $\alpha > 1$ , the gain term increases rapidly with  $N$ , indicating that the larger  $\alpha$  is, the more advantageous segmentation becomes.

**Theorem 1** (Advantage of Divide-and-Conquer). *Let the intrinsic error rate  $\beta_0 > 0$  and the correlation amplification factor  $\alpha > 1$ , and fix the integer  $k \geq 2$ . Under the empirical scaling law*

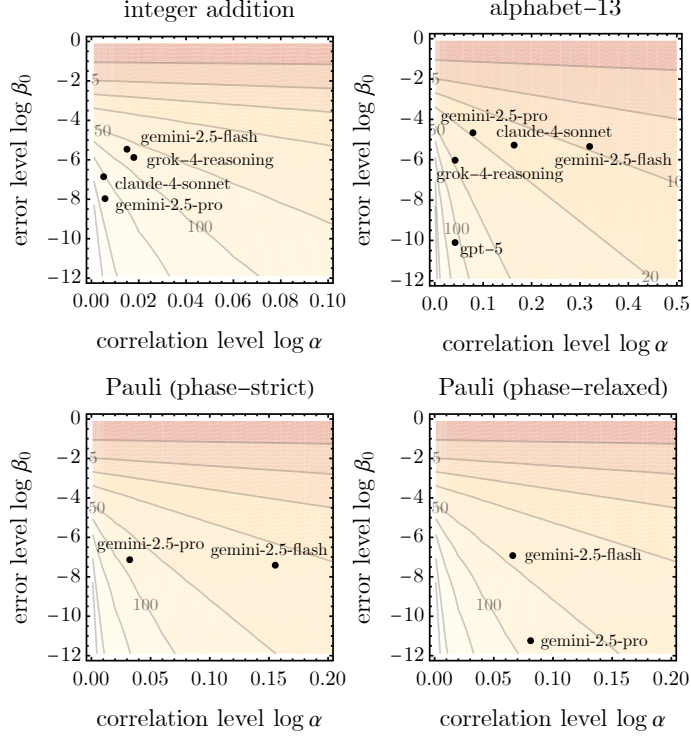


Figure 7: Correlation–error map grouped by task, with color indicating the value of  $\log N_*$ . The horizontal and vertical axes,  $(\log \alpha, \log \beta_0)$ , represent the correlation level and error level, respectively. The gray contour line and the numbers along it denote the sequence length  $N$ .

$\text{SAR}(N) = \exp[-\beta_0 N \alpha^{N-1}]$ , for the segmentation into  $k$  equal sub-tasks to yield a positive gain  $\Delta(N, k) > 0$ , it would be sufficient if the sequence length exceeds the following bound

$$N \geq N_{\text{DC}} = 1 + \frac{1}{\log \alpha} \left( \log \left( 1 - \frac{2 \log \theta_{N,k}}{\beta_0} \right) + \frac{\log 2}{1 - 1/k} \right), \quad (24)$$

meaning that for all  $N \geq N_{\text{DC}}$ , one has  $\text{SAR}_{\text{DC}}(N, k) > \text{SAR}(N)$ .

(See App. C for a proof.)

This result provides an explicit criterion for when the divide-and-conquer approach is beneficial. Under this strategy, as evident from Eq. (22), the intrinsic error rate  $\beta_0$  remains unchanged, while the correlation amplification factor  $\alpha$  is effectively rescaled to  $\alpha_{\text{eff}} \simeq \alpha^{1/k}$  in the large- $N$  regime. As a consequence, the characteristic accuracy-cliff scale is extended to

$$N_* \simeq 1 + \frac{\log(1/\beta_0)}{\log \alpha_{\text{eff}}} = 1 + k \frac{\log(1/\beta_0)}{\log \alpha}, \quad (25)$$

growing approximately linearly with  $k$ , according to Eq. (15). The empirical effectiveness of the divide-and-conquer strategy is demonstrated in Fig. 8, where the linear- $k$  scaling of accuracy cliff is indeed observed.

In summary, the empirical scaling law does more than describe the accuracy cliff—it also *predicts how to mitigate it*: segmentation effectively reduces the compounding of correlated errors and extends the *reliable length scale* of LLMs by roughly a factor of  $k$ , transforming an observed limitation into a quantitative improvement strategy.

## 5 Related Works

**Single-pass reasoning and capacity limits.** Recent research has shown that even when models can locally apply correct reasoning steps, global accuracy collapses as reasoning chains lengthen. This

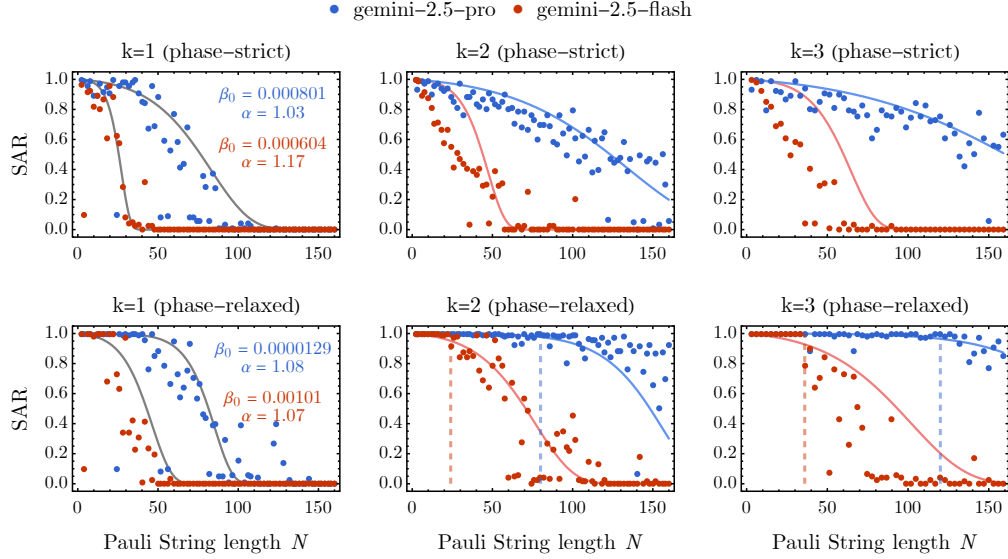


Figure 8: Divide-and-conquer evaluation on the Pauli string multiplication task under both phase-restricted and phase-relaxed criteria, using `gemini-2.5-flash` and `gemini-2.5-pro`. The gray  $k=1$  curves show the fitted  $\text{SAR}(N)$  from Eq. (14); the extracted  $(\alpha, \beta_0)$  values are then used to plot the theoretical  $\text{SAR}(N/k)^k$  curves for  $k=2$  and  $k=3$  (red and blue), assuming no overhead ( $\theta_{N,k} = 1$ ). In the phase-restricted case, the pro model closely follows the predicted improvement, while the flash model performs below the theoretical curves, due to additional overhead in divide and combine. In the phase-relaxed case, both models closely follow the predicted improvement, and additionally expand the perfect-accuracy plateau by approximately a factor of  $k$  (indicated by the colored dashed lines).

phenomenon parallels information-theoretic capacity limits of single forward passes. The *Fano-style upper bound* framework [Wan et al., 2025a] formalizes this collapse for multi-hop question answering (MHQA), proving that once task complexity exceeds the model’s per-pass information capacity, accuracy must drop sharply—mirroring our empirical SAR crossover. Their work interprets the reasoning chain as a noisy communication channel, bounded by mutual information, while our SAR analysis arrives at the same breakdown curve from a statistical-physics viewpoint, emphasizing the all-to-all error propagation in the attention architecture as the key underlying mechanism. Together they highlight the inevitability of reliability loss in single-pass reasoning under finite model capacity.

**Prompting paradigms and decomposition.** A wide range of prompting methods—Direct prompting, Chain-of-Thought (CoT) [Wei et al., 2022, Kojima et al., 2022], ReAct [Yao et al., 2023], Plan-and-Solve [Wang et al., 2023], and Self-Ask [Press et al., 2023]—operate in the *single-pass* regime, assuming the full reasoning chain fits within one generation. By contrast, *multi-call* frameworks such as Self-Refine [Madaan et al., 2023], InfoQA [Wan et al., 2025a], and agentic systems for programming or reasoning [Li et al., 2024, Qian et al., 2024, Kim et al., 2024] mitigate this bottleneck by decomposing reasoning into smaller, verifiable subcalls. Our SAR-based analysis provides a quantitative explanation of why such multi-call methods succeed: by resetting the error accumulation process, they effectively bound per-step complexity below the model’s capacity threshold, preventing the exponential or super-exponential degradation seen in single-pass reasoning.

**Self-checking, verification, and robust reasoning.** Other orthogonal strategies—such as self-consistency sampling, debate-style verification, and tool-augmented reasoning—attempt to mitigate compounding errors by introducing redundancy or external validation [Yao et al., 2023, Xie et al., 2025, Wan et al., 2025b, McCoy et al., 2023]. SAR offers a unified diagnostic lens for such methods: improved reliability corresponds to reduced intrinsic error rate  $\beta_0$ , while better verification or decomposition corresponds to smaller accumulation factor  $\alpha$ . Thus, SAR quantitatively links algorithmic interventions to empirical stability regimes.

## 6 Conclusion and Future Work

We introduced the *Sequence Accuracy Rate (SAR)* as a principled metric for quantifying reliability in deterministic reasoning tasks performed by large language models. Through three controlled benchmarks—cyclic letter replacement, integer addition, and Pauli string multiplication—we demonstrated that SAR provides a quantitative view of how local inaccuracies compound with sequence length. Empirical results reveal a sharp reliability crossover rather than a simple exponential decay, indicating correlated error accumulation rather than independent token noise.

To explain this behavior, we developed a statistical-physics model inspired by the Sherrington–Kirkpatrick spin-glass system, linking empirical scaling parameters to interpretable quantities: intrinsic error rate  $\beta_0$  and error accumulation strength  $\alpha$ . This hypothetical model connects observed *accuracy cliffs* in deterministic reasoning to correlated interactions within LLMs.

Future directions include extending SAR to stochastic reasoning pipelines, integrating it with self-verification or multi-call decomposition schemes, and applying the statistical-physics approach to study model scaling laws and architectural modifications. More broadly, SAR provides a foundation for treating reasoning reliability as a measurable and scalable property, enabling systematic analysis and engineering of models that sustain compositional accuracy over increasing complexity.

## 7 Acknowledgment

We would like to thank Chen Nie for the engineering support. We would like to acknowledge helpful discussion with Victor Albert and Hsin-Yuan Huang on bench.science. W.H. additionally thanks Tianxiao Hu for helpful discussions.

## References

- Pietro Astolfi, Marlene Careil, Melissa Hall, Oscar Mañas, Matthew Muckley, Jakob Verbeek, Adriana Romero Soriano, and Michal Drozdal. Consistency-diversity-realism pareto fronts of conditional image generative models. *arXiv preprint arXiv:2406.10429*, 2024.
- Karl Cobbe, Vineet Kosaraju, Mohammad Bavarian, Mark Chen, Heewoo Jun, Lukasz Kaiser, Matthias Plappert, Jerry Tworek, Jacob Hilton, Reiichiro Nakano, et al. Training verifiers to solve math word problems. *arXiv preprint arXiv:2110.14168*, 2021.
- Alexander Havrilla, Sharath Chandra Raparthy, Christoforos Nalmpantis, Jane Dwivedi-Yu, Maksym Zhuravinskiy, Eric Hambro, and Roberta Raileanu. Glore: When, where, and how to improve llm reasoning via global and local refinements. In *International Conference on Machine Learning*, pages 17719–17733. PMLR, 2024.
- Dan Hendrycks, Collin Burns, Saurav Kadavath, Akul Arora, Steven Basart, Eric Tang, Dawn Song, and Jacob Steinhardt. Measuring mathematical problem solving with the math dataset. *arXiv preprint arXiv:2103.03874*, 2021.
- Sehoon Kim, Suhong Moon, Ryan Tabrizi, Nicholas Lee, Michael W Mahoney, Kurt Keutzer, and Amir Gholami. An llm compiler for parallel function calling. In *International Conference on Machine Learning*, pages 24370–24391. PMLR, 2024.
- Takeshi Kojima, Shixiang Shane Gu, Machel Reid, Yutaka Matsuo, and Yusuke Iwasawa. Large language models are zero-shot reasoners. *Advances in neural information processing systems*, 35: 22199–22213, 2022.
- Brenden Lake and Marco Baroni. Generalization without systematicity: On the compositional skills of sequence-to-sequence recurrent networks. In *International conference on machine learning*, pages 2873–2882. PMLR, 2018.
- Aitor Lewkowycz, Anders Andreassen, David Dohan, Ethan Dyer, Henryk Michalewski, Vinay Ramasesh, Ambrose Slone, Cem Anil, Imanol Schlag, Theo Gutman-Solo, et al. Solving quantitative reasoning problems with language models. *Advances in neural information processing systems*, 35:3843–3857, 2022.

- Xinyi Li, Sai Wang, Siqi Zeng, Yu Wu, and Yi Yang. A survey on llm-based multi-agent systems: workflow, infrastructure, and challenges. *Vicinagearth*, 1(1):9, 2024.
- Percy Liang, Rishi Bommasani, Tony Lee, Dimitris Tsipras, Dilara Soylu, Michihiro Yasunaga, Yian Zhang, Deepak Narayanan, Yuhuai Wu, Ananya Kumar, et al. Holistic evaluation of language models. *arXiv preprint arXiv:2211.09110*, 2022.
- Chin-Yew Lin. ROUGE: A package for automatic evaluation of summaries. In *Text Summarization Branches Out*, pages 74–81, Barcelona, Spain, July 2004. Association for Computational Linguistics. URL <https://aclanthology.org/W04-1013/>.
- Nelson F Liu, Kevin Lin, John Hewitt, Ashwin Paranjape, Michele Bevilacqua, Fabio Petroni, and Percy Liang. Lost in the middle: How language models use long contexts. *arXiv preprint arXiv:2307.03172*, 2023.
- Aman Madaan, Niket Tandon, Prakhar Gupta, Skyler Hallinan, Luyu Gao, Sarah Wiegrefe, Uri Alon, Nouha Dziri, Shrimai Prabhumoye, Yiming Yang, et al. Self-refine: Iterative refinement with self-feedback. *Advances in Neural Information Processing Systems*, 36:46534–46594, 2023.
- R Thomas McCoy, Shunyu Yao, Dan Friedman, Matthew Hardy, and Thomas L Griffiths. Embers of autoregression: Understanding large language models through the problem they are trained to solve. *arXiv preprint arXiv:2309.13638*, 2023.
- Kishore Papineni, Salim Roukos, Todd Ward, and Wei-Jing Zhu. Bleu: a method for automatic evaluation of machine translation. In Pierre Isabelle, Eugene Charniak, and Dekang Lin, editors, *Proceedings of the 40th Annual Meeting of the Association for Computational Linguistics*, pages 311–318, Philadelphia, Pennsylvania, USA, July 2002. Association for Computational Linguistics. doi: 10.3115/1073083.1073135. URL <https://aclanthology.org/P02-1040/>.
- Ofir Press, Muru Zhang, Sewon Min, Ludwig Schmidt, Noah A Smith, and Mike Lewis. Measuring and narrowing the compositionality gap in language models. In *Findings of the Association for Computational Linguistics: EMNLP 2023*, pages 5687–5711, 2023.
- Chen Qian, Wei Liu, Hongzhang Liu, Nuo Chen, Yufan Dang, Jiahao Li, Cheng Yang, Weize Chen, Yusheng Su, Xin Cong, et al. Chatdev: Communicative agents for software development. In *Proceedings of the 62nd Annual Meeting of the Association for Computational Linguistics (Volume 1: Long Papers)*, pages 15174–15186, 2024.
- Miles Turpin, Julian Michael, Ethan Perez, and Samuel Bowman. Language models don’t always say what they think: Unfaithful explanations in chain-of-thought prompting. *Advances in Neural Information Processing Systems*, 36:74952–74965, 2023.
- Kaiyang Wan, Lang Gao, Honglin Mu, Preslav Nakov, Yuxia Wang, and Xiuying Chen. A fano-style accuracy upper bound for llm single-pass reasoning in multi-hop qa. *arXiv preprint arXiv:2509.21199*, 2025a.
- Kaiyang Wan, Honglin Mu, Rui Hao, Haoran Luo, Tianle Gu, and Xiuying Chen. A cognitive writing perspective for constrained long-form text generation. *arXiv preprint arXiv:2502.12568*, 2025b.
- Lei Wang, Wanyu Xu, Yihuai Lan, Zhiqiang Hu, Yunshi Lan, Roy Ka-Wei Lee, and Ee-Peng Lim. Plan-and-solve prompting: Improving zero-shot chain-of-thought reasoning by large language models. In *Proceedings of the 61st Annual Meeting of the Association for Computational Linguistics (Volume 1: Long Papers)*, pages 2609–2634, 2023.
- Xuezhi Wang, Jason Wei, Dale Schuurmans, Quoc Le, Ed Chi, Sharan Narang, Aakanksha Chowdhery, and Denny Zhou. Self-consistency improves chain of thought reasoning in language models. *arXiv preprint arXiv:2203.11171*, 2022.
- Jason Wei, Xuezhi Wang, Dale Schuurmans, Maarten Bosma, Fei Xia, Ed Chi, Quoc V Le, Denny Zhou, et al. Chain-of-thought prompting elicits reasoning in large language models. *Advances in neural information processing systems*, 35:24824–24837, 2022.

Zhuohan Xie, Rui Xing, Yuxia Wang, Jiahui Geng, Hasan Iqbal, Dhruv Sahnan, Iryna Gurevych, and Preslav Nakov. Fire: Fact-checking with iterative retrieval and verification. In *Findings of the Association for Computational Linguistics: NAACL 2025*, pages 2901–2914, 2025.

Shunyu Yao, Jeffrey Zhao, Dian Yu, Nan Du, Izhak Shafran, Karthik Narasimhan, and Yuan Cao. React: Synergizing reasoning and acting in language models. In *International Conference on Learning Representations (ICLR)*, 2023.

## A Success Rate Analysis of Pauli String test

Suppose an intellectual agent attempts to compute the product of two Pauli strings of length  $N$ . At each site, two types of operations are required:

1. A *Pauli multiplication step*, where  $P_i \times Q_i$  is reduced to a Pauli operator  $R_i$  and a local phase factor  $\phi_i$ . Let the probability of correctly performing this step be  $p_\sigma$ .
2. A *phase multiplication step*, where the accumulated phase is updated as  $\Phi \mapsto \Phi \times \phi_i$ . Let the probability of correctly performing a single phase update be  $p_\phi$ .

We first model the accumulated phase as a Markov chain on the cyclic group  $G = \{1, i, -1, -i\}$  with the state order  $(1, i, -1, -i)$ . At each step, the algorithm multiplies the current phase by one of the group elements, but due to noise it returns an incorrect element with probability  $p_\phi$ , and the correct (true) element with probability  $1 - p_\phi$ . Hence, each of the three incorrect elements occurs with probability  $\frac{p_\phi}{3}$ . Let  $\mathbb{1}$  denote the  $4 \times 4$  identity matrix and  $J$  the all-ones matrix. When the intended multiplier is 1, the one-step transition kernel is the circulant matrix

$$K = (1 - p_\phi) \mathbb{1} + \frac{p_\phi}{3} (J - \mathbb{1}). \quad (26)$$

Define the four permutation (left-shift) matrices  $\{S_\phi : \phi \in G\}$  that implement left multiplication by  $\phi$  on the state order; explicitly,

$$S_1 = \mathbb{1}, \quad S_i = \begin{bmatrix} 0 & 0 & 0 & 1 \\ 1 & 0 & 0 & 0 \\ 0 & 1 & 0 & 0 \\ 0 & 0 & 1 & 0 \end{bmatrix}, \quad S_{-1} = \begin{bmatrix} 0 & 0 & 1 & 0 \\ 0 & 0 & 0 & 1 \\ 1 & 0 & 0 & 0 \\ 0 & 1 & 0 & 0 \end{bmatrix}, \quad S_{-i} = \begin{bmatrix} 0 & 1 & 0 & 0 \\ 0 & 0 & 0 & 1 \\ 0 & 0 & 1 & 0 \\ 1 & 0 & 0 & 0 \end{bmatrix}.$$

Thus, if the multiplier at a step is  $\phi \in G$ , the corresponding one-step transition matrix is

$$T(\phi) = S_\phi K. \quad (27)$$

Because every permutation matrix commutes with  $K$ , i.e.  $S_\phi K = K S_\phi, \forall \phi \in G$ , the product of step-wise transitions reduces to a similarity transform. For any sequence of true multipliers  $\phi_1, \dots, \phi_N$ , we have

$$T(\phi_N) \cdots T(\phi_1) = (S_{\phi_N} \cdots S_{\phi_1}) K^N = S_\Phi K^N, \quad \Phi := \phi_N \cdots \phi_1. \quad (28)$$

Therefore, the success rate of phase computing task is given by:

$$P_\phi(N) = e_\Phi^\top S_\Phi K^N e_1, \quad (29)$$

where  $e_\Phi$  is the basis vector of  $\Phi$  in the state order  $(1, i, -1, -i)$  and  $K^N = \frac{1}{4}J + \left(\frac{3-4p_\phi}{3}\right)^N (\mathbb{1} - \frac{1}{4}J)$ . Explicitly, this gives:

$$P_\phi(N) = \frac{1}{4} + \frac{3}{4} \left(\frac{3-4p_\phi}{3}\right)^N. \quad (30)$$

Combining this with the individual Pauli multiplication success rate, the overall sequence accuracy rate is

$$\text{SAR}(N) = (1 - p_\sigma)^N \left[ \frac{1}{4} + \frac{3}{4} \left(\frac{3-4p_\phi}{3}\right)^N \right]. \quad (31)$$

The requirement to accumulate local phase factors across all sites is especially instructive, as it directly reflects the need for *memory handling* in agent design: just as an LLM must correctly maintain and update a state variable across multiple reasoning steps, the phase register here must be updated consistently at every site.

## B Modeling the LLM SAR with SK-Model

In this appendix, we propose and solve a minimal energy-based toy model that captures the empirical scaling behavior in Eq. (14) and offers a possible physical interpretation of its underlying mechanism.

Let  $\mathcal{D} = \{(x_{(k)}, y_{(k)})\}_{k=1}^K$  be a dataset consisting of input–output sequence pairs, where each input sequence  $x_{(k)}$  is deterministically mapped to a unique correct output sequence  $y_{(k)}$ . An LLM trained on this dataset defines a conditional probability distribution  $p_\theta(y | x)$  over output sequences.

### B.1 Definitions and independent-token baseline

The *Sequence Accuracy Rate (SAR)* is defined as the geometric mean of the model’s probability on correct sequences:

$$\text{SAR}(p_\theta; \mathcal{D}) = \exp\left(\frac{1}{K} \sum_{k=1}^K \log p_\theta(y_{(k)} | x_{(k)})\right) \in (0, 1]. \quad (32)$$

Introduce Ising variables for correctness:

$$s_i = \begin{cases} +1, & y_i \text{ is correct,} \\ -1, & \text{otherwise,} \end{cases} \quad s = (s_1, \dots, s_N) \in \{\pm 1\}^N,$$

so all-correct output sequence corresponds to  $s_i = +1$  for all  $i = 1, \dots, N$ , which we denote jointly as  $s = \mathbf{1}$ . If each token were generated independently with a token-level accuracy rate  $p_{\text{tok}}$ , the expected sequence accuracy would scale as

$$\text{SAR} = p_{\text{tok}}^N, \quad (33)$$

which decays exponentially with sequence length  $N$ . The corresponding energy model for the Ising variables is simply

$$E[s] = -h \sum_{i=1}^N s_i, \quad (34)$$

such that

$$\text{SAR} = \frac{e^{-E[s=\mathbf{1}]}}{\sum_s e^{-E[s]}} = \left(\frac{1}{1 + e^{-2h}}\right)^N, \quad (35)$$

implying that the external field  $h$  parameterizes the token-level accuracy as

$$p_{\text{tok}} = \frac{1}{1 + e^{-2h}}. \quad (36)$$

However, this independent-token prediction fails to capture the crossover behavior observed in experiments.

### B.2 Energy model (Sherrington–Kirkpatrick (SK) Hamiltonian)

In our experiments, the Sequence Accuracy Rate (SAR) shows a pronounced dependence on output length  $N$ . While one might expect a simple exponential decay,  $\text{SAR} \sim e^{-\alpha N}$ , our results reveal a clear *accuracy cliff*: SAR remains high for short sequences, then sharply declines around a characteristic length. This behavior indicates that sequence-level reliability in LLMs arises not from independent token errors but from correlated or scale-dependent effects, such as contextual coupling and calibration across sequence lengths, governing the shift from reliable to unreliable generation in deterministic tasks. We hypothesize that the deviation arises from all-to-all correlations among tokens during sequence generation. The self-attention mechanism in LLMs inherently couples every token to every other token, introducing dependencies beyond the independent-token picture. These correlations are not purely constructive: noise, interference, or internal competition within the network can generate effective random coupling strengths  $J_{ij}$  between the Ising variables  $s_i$  (the token correctness labels). Such couplings modify the collective statistics of sequence correctness, producing a non-exponential decay and the observed crossover in SAR.

We therefore propose the following energy model:

$$E_J[s] = - \sum_{i < j} J_{ij} s_i s_j - h \sum_{i=1}^N s_i, \quad (37)$$

where  $s_i = \pm 1$  for  $i = 1, 2, \dots, N$  are Ising variables representing the correctness of the  $i$ -th token  $y_i$  in the output sequence generated by the LLM.

The coupling strengths  $J_{ij}$  are drawn independently from a Gaussian distribution with zero mean and finite variance:

$$\mathbb{E}_J[J_{ij}] = 0, \quad \mathbb{E}_J[J_{ij}^2] = J_0^2. \quad (38)$$

They model the noisy all-to-all correlations in token generation, and  $J_0$  characterizes the noise strength, which is assumed to be weak. The external field  $h$  parameterizes the token-level accuracy rate via Eq. (0): a strong field  $h$  corresponds to a high token-level accuracy, which is typically assumed. This model is equivalent to the well-known *Sherrington–Kirkpatrick (SK) model* in spin-glass physics.

For a particular random realization of  $J_{ij}$ , the probability of observing the Ising sequence  $s$  is

$$p_J[s] = \frac{1}{Z_J} e^{-E_J[s]}, \quad (39)$$

where  $Z_J$  is the partition function,

$$Z_J = \sum_s e^{-E_J[s]}. \quad (40)$$

Specifically, the Sequence Accuracy Rate (SAR) corresponds to the geometric mean probability of the all-correct configuration under random couplings:

$$\text{SAR} := \exp(\mathbb{E}_J \log p_J[s = \mathbf{1}]). \quad (41)$$

### B.3 Replica trick and disorder average

From Eq. (41), it is straightforward to show that

$$\begin{aligned} \log \text{SAR} &= \mathbb{E}_J \log p_J[s = \mathbf{1}] = \mathbb{E}_J \log \left( \frac{e^{-E_J[s=\mathbf{1}]}}{Z_J} \right) \\ &= \mathbb{E}_J \left( -E_J[s = \mathbf{1}] - \log Z_J \right) = \mathbb{E}_J \left( \sum_{i < j} J_{ij} + hN - \log Z_J \right). \end{aligned} \quad (42)$$

Using the disorder mean  $\mathbb{E}_J[J_{ij}] = 0$ , we have

$$\log \text{SAR} = hN - \mathbb{E}_J \log Z_J. \quad (43)$$

**Replica trick.** The expectation  $\mathbb{E}_J \log Z_J$  in (43) is intractable directly. Physicists therefore use the *replica trick*:

$$\mathbb{E}_J \log Z_J = \lim_{n \rightarrow 0} \partial_n \mathbb{E}_J [Z_J^n]. \quad (44)$$

By definition,

$$\begin{aligned} \mathbb{E}_J [Z_J^n] &= \mathbb{E}_J \left[ \left( \sum_{[s]} \exp \left( \sum_{i < j} J_{ij} s_i s_j + h \sum_i s_i \right) \right)^n \right] \\ &= \sum_{\{s^a\}} \exp \left( \sum_{a=1}^n \sum_{i < j} J_{ij} s_i^a s_j^a + h \sum_{a=1}^n \sum_{i=1}^N s_i^a \right), \end{aligned} \quad (45)$$

where the spin variables have been replicated to  $s_i^a$  with  $i = 1, \dots, N$  and  $a = 1, \dots, n$ . Here  $N$  is the number of sites (sequence length) and  $n$  the number of replicas.

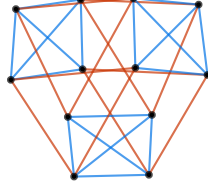


Figure 9: Example:  $K_4 \times K_3$  graph.

**Disorder average.** Averaging  $Z_J^n$  over i.i.d. Gaussian couplings  $J_{ij}$  with  $\mathbb{E}_J[J_{ij}] = 0$ ,  $\mathbb{E}_J[J_{ij}^2] = J_0^2$ , we obtain

$$\begin{aligned} \mathbb{E}_J[Z_J^n] &= \sum_{\{s^a\}} \prod_{i < j} \mathbb{E}_{J_{ij}} \exp\left(\sum_{a=1}^n J_{ij} s_i^a s_j^a\right) \exp\left(h \sum_{a=1}^n \sum_{i=1}^N s_i^a\right) \\ &= \sum_{\{s^a\}} \prod_{i < j} \exp\left(\frac{J_0^2}{2} C_{ij}^2\right) \exp\left(h \sum_{a=1}^n \sum_{i=1}^N s_i^a\right), \end{aligned} \quad (46)$$

where  $C_{ij} \equiv \sum_{a=1}^n s_i^a s_j^a$  and we used the Gaussian moment-generating function  $\mathbb{E}_{J_{ij}} e^{J_{ij} C_{ij}} = \exp\left(\frac{J_0^2}{2} C_{ij}^2\right)$ . Thus,

$$\begin{aligned} \mathbb{E}_J[Z_J^n] &= \sum_{\{s^a\}} \exp\left(\frac{J_0^2}{2} \sum_{i < j} C_{ij}^2 + h \sum_{a=1}^n \sum_{i=1}^N s_i^a\right) \\ &= \sum_{\{s^a\}} \exp\left(\frac{J_0^2}{2} \sum_{i < j} \left(\sum_{a=1}^n s_i^a s_j^a\right)^2 + h \sum_{a=1}^n \sum_{i=1}^N s_i^a\right). \end{aligned} \quad (47)$$

Expanding the quadratic replica term gives

$$\begin{aligned} \sum_{i < j} \left(\sum_{a=1}^n s_i^a s_j^a\right)^2 &= \sum_{i < j} \left(\sum_{a=1}^n (s_i^a s_j^a)^2 + 2 \sum_{a < b} s_i^a s_j^a s_i^b s_j^b\right) \\ &= \sum_{i < j} \left(n + 2 \sum_{a < b} s_i^a s_j^a s_i^b s_j^b\right) \\ &= \frac{nN(N-1)}{2} + 2 \sum_{i < j} \sum_{a < b} s_i^a s_j^a s_i^b s_j^b. \end{aligned} \quad (48)$$

Introducing the constant  $\Omega \equiv \exp(J_0^2 N(N-1)/4)$  to absorb the  $\mathcal{O}(n)$  term, we obtain the compact form

$$\mathbb{E}_J[Z_J^n] = \Omega^n \sum_{\{s^a\}} \exp\left(J_0^2 \sum_{i < j} \sum_{a < b} s_i^a s_j^a s_i^b s_j^b + h \sum_{a=1}^n \sum_{i=1}^N s_i^a\right). \quad (49)$$

**Geometric interpretation.** Equation (49) defines a plaquette four-spin interaction on the graph product  $K_N \times K_n$  (complete graphs on  $N$  and  $n$  vertices, respectively). The construction is self-dual under the exchange  $N \leftrightarrow n$ .

### B.3.1 Small- $J_0$ Expansion

Assuming that the noise strength  $J_0$  is weak, we perform a perturbative expansion of the replicated partition function in powers of  $J_0$ :

$$\mathbb{E}_J Z_J^n = \Omega^n \sum_{\{s\}} e^{h \sum_{i,a} s_i^a} \left[ 1 + J_0^2 \sum_{i < j, a < b} s_i^a s_j^a s_i^b s_j^b + \frac{J_0^4}{2} \left( \sum_{i < j, a < b} s_i^a s_j^a s_i^b s_j^b \right)^2 + \dots \right]. \quad (50)$$

Because the Boltzmann factor factorizes over spins,

$$e^{h \sum_{i,a} s_i^a} = \prod_{i,a} e^{h s_i^a},$$

the spin summations can be carried out independently. For a single spin, we define

$$z := \sum_{s=\pm 1} e^{hs} = 2 \cosh h, \quad m := \langle s \rangle = \frac{1}{z} \sum_{s=\pm 1} s e^{hs} = \tanh h. \quad (51)$$

Hence, after performing the average over independent spins,

$$\begin{aligned} \mathbb{E}_J Z_J^n &= \Omega^n z^{nN} \left[ 1 + \frac{J_0^2}{4} N(N-1)n(n-1)m^4 \right. \\ &\quad \left. + \frac{J_0^4}{2} N(N-1)n(n-1) \left( \frac{1}{4} + \frac{1}{2}(N+n-4)m^4 + (N-2)(n-2)m^6 + \right. \right. \end{aligned} \quad (52)$$

$$\left. \left. \frac{1}{4} \left( \frac{1}{4} N(N-1)n(n-1) - (2N-3)(2n-3) \right) m^8 \right) + \dots \right]. \quad (53)$$

**Plaquette pairings.** The term

$$\left\langle \sum_{i < j, a < b} s_i^a s_j^a s_i^b s_j^b \right\rangle = \frac{1}{4} N(N-1)n(n-1)m^4$$

counts the number of plaquettes on the product graph  $K_N \times K_n$ , corresponding to choosing one edge from  $K_N$  and one from  $K_n$  independently. Each summand represents a single four-spin plaquette interaction.

At order  $J_0^4$ , we must evaluate  $\left\langle \left( \sum_{i < j, a < b} s_i^a s_j^a s_i^b s_j^b \right)^2 \right\rangle$ , which decomposes into five distinct topological classes of plaquette pairings:

- (A) Double-covered plaquettes:  $\frac{1}{4} N(N-1)n(n-1)$ .
- (B) Edge-sharing plaquette pairs (sharing a  $K_n$  edge):  $\frac{1}{2} N(N-1)(N-2)n(n-1)m^4$ .
- (B') Edge-sharing plaquette pairs (sharing a  $K_N$  edge):  $\frac{1}{2} N(N-1)n(n-1)(n-2)m^4$ .
- (C) Corner-sharing plaquette pairs:  $N(N-1)(N-2)n(n-1)(n-2)m^6$ .
- (D) Non-intersecting plaquette pairs:  $\frac{1}{4} N(N-1)n(n-1) \left[ \frac{1}{4} N(N-1)n(n-1) - (2N-3)(2n-3) \right] m^8$ .

The sum of all classes yields

$$\begin{aligned} \left\langle \left( \sum_{i < j, a < b} s_i^a s_j^a s_i^b s_j^b \right)^2 \right\rangle &= N(N-1)n(n-1) \left[ \frac{1}{4} + \frac{1}{2}(N+n-4)m^4 + (N-2)(n-2)m^6 \right. \\ &\quad \left. + \frac{1}{4} \left( \frac{1}{4} N(N-1)n(n-1) - (2N-3)(2n-3) \right) m^8 \right]. \end{aligned} \quad (54)$$

Substituting (54) into (53) gives the final expansion

$$\begin{aligned} \mathbb{E}_J Z_J^n &= \Omega^n (2 \cosh h)^{nN} \left[ 1 + \frac{J_0^2}{4} N(N-1)n(n-1)m^4 \right. \\ &\quad \left. + \frac{J_0^4}{2} N(N-1)n(n-1) \left( \frac{1}{4} + \frac{1}{2}(N+n-4)m^4 + (N-2)(n-2)m^6 + \right. \right. \end{aligned} \quad (55)$$

$$\left. \left. \frac{1}{4} \left( \frac{1}{4} N(N-1)n(n-1) - (2N-3)(2n-3) \right) m^8 \right) + \dots \right]. \quad (56)$$

**Replica limit.** Taking the replica limit as in Eq. (44),

$$\begin{aligned} \mathbb{E}_J \log Z_J &= \lim_{n \rightarrow 0} \partial_n \mathbb{E}_J Z_J^n \\ &= \log \Omega + N \log(2 \cosh h) - \frac{J_0^2}{4} N(N-1)m^4 \\ &\quad - \frac{J_0^4}{2} N(N-1) \left[ \frac{1}{4} + \frac{1}{2}(N-4)m^4 - 2(N-2)m^6 + \frac{3}{4}(2N-3)m^8 \right] + \mathcal{O}(J_0^6). \end{aligned} \quad (57)$$

**Result for SAR.** Substituting (57) into Eq. (43) yields

$$\begin{aligned} \log \text{SAR} &= N(h - \log(2 \cosh h)) + \frac{J_0^2}{4} N(N-1)(-1 + \tanh^4 h) \\ &+ \frac{J_0^4}{2} N(N-1) \left[ -\frac{1}{2} - (N-4) \tanh^4 h + 4(N-2) \tanh^6 h - \frac{3}{2}(2N-3) \tanh^8 h \right] + \mathcal{O}(J_0^6). \end{aligned} \quad (58)$$

For  $h \gg 1$ , using  $\tanh h \approx 1 - 2e^{-2h}$ ,

$$\log \text{SAR} \simeq -e^{-2h} N \left[ 1 + 2J_0^2(N-1) + 2J_0^4(N-1)^2 + \mathcal{O}(J_0^6) \right]. \quad (59)$$

Motivated by the expansion above, an empirical expression that reproduces the observed crossover behavior is

$$\text{SAR}(N) = \exp\left(-N \exp\left[\frac{2J_0^2}{1+2J_0}(N-1) - 2h\right]\right), \quad (60)$$

which provides a good approximation over a broad range of  $J_0$  for sufficiently large  $h$ .

## C Proof of Theorem 1

*Proof.* Start with the condition

$$N \geq N_{\text{DC}} = 1 + \frac{1}{\log \alpha} \left( \log \left( 1 - \frac{2 \log \theta_{N,k}}{\beta_0} \right) + \frac{\log 2}{1-1/k} \right), \quad (61)$$

with  $\alpha > 1$ ,  $\beta_0 > 0$ ,  $0 < \theta_{N,k} \leq 1$ ,  $k \geq 2$ . Each term in  $N_{\text{DC}}$  is non-negative,

$$\log \alpha > 0, \quad \log \left( 1 - \frac{2 \log \theta_{N,k}}{\beta_0} \right) \geq 0, \quad \frac{\log 2}{1-1/k} > 0, \quad (62)$$

therefore Eq. (61) implies the following weaker conditions:

$$N > 1, \quad (63)$$

$$N > 1 + \frac{1}{\log \alpha} \log \left( 1 - \frac{2 \log \theta_{N,k}}{\beta_0} \right) > 1 + \frac{1}{\log \alpha} \log \left( -\frac{2 \log \theta_{N,k}}{\beta_0} \right), \quad (64)$$

$$N > \frac{1}{\log \alpha} \frac{\log 2}{1-1/k}, \quad (65)$$

which are nevertheless more directly useful.

Eq. (65) implies

$$\begin{aligned} &N(1-1/k) \log \alpha > \log 2 \\ \Rightarrow &\alpha^{N(1-1/k)} > 2 \\ \Rightarrow &\alpha^{-N(1-1/k)} < 1/2 \\ \Rightarrow &(1 - \alpha^{N/k-N}) > 1/2. \end{aligned} \quad (66)$$

Eq. (64) implies

$$(N-1) \log \alpha > \log \left( -\frac{2 \log \theta_{N,k}}{\beta_0} \right) \Rightarrow \frac{1}{2} \beta_0 \alpha^{N-1} > -\log \theta_{N,k}. \quad (67)$$

Putting Eqs. (63), (66), (67) together, we have

$$\begin{aligned} \beta_0 N (\alpha^{N-1} - \alpha^{N/k-1}) &= \beta_0 \alpha^{N-1} N (1 - \alpha^{N/k-N}) \\ &> \beta_0 \alpha^{N-1} \times 1 \times \frac{1}{2} \\ &> -\log \theta_{N,k}, \end{aligned} \quad (68)$$

therefore the logarithmic gain  $\Delta(N, k) = \log \theta_{N,k} + \beta_0 N (\alpha^{N-1} - \alpha^{N/k-1}) > 0$  is positive.  $\square$